LETTER • OPEN ACCESS

Are microtubules electron-based topological insulators?

To cite this article: Varsha Subramanyan *et al* 2023 *EPL* **143** 46001

A Letters Journal Exploring the Frontiers of Physics

August 2023

EPL, **143** (2023) 46001
doi: 10.1209/0295-5075/acec94

www.epljournal.org

Are microtubules electron-based topological insulators?

Varsha Subramanyan[1(a)], Kay L. Kirkpatrick[2,1], Saraswathi Vishveshwara[3] and Smitha Vishveshwara[1(b)]

[1] *Department of Physics, University of Illinois - Urbana-Champaign, IL, USA*
[2] *Department of Mathematics, University of Illinois - Urbana-Champaign, IL, USA*
[3] *Molecular Biophysics Unit, Indian Institute of Science - Bengaluru, India*

received 3 April 2023; accepted in final form 2 August 2023
published online 15 August 2023

Abstract – A microtubule is a cylindrical biological polymer that plays key roles in cellular structure, transport, and signalling. In this work, based on studies of electronic properties of polyacetelene and mechanical properties of microtubules themselves (Spakowitz A. J., *Phys. Rev. Lett.*, **103** (2009) 248101), we explore the possibility that microtubules could act as topological insulators that are gapped to electronic excitations in the bulk but possess robust electronic bounds states at the tube ends. Through analyses of structural and electronic properties, we model the microtubule as a cylindrical stack of Su-Schrieffer-Heeger chains (originally proposed in the context of polyacetylene) describing electron hopping between the underlying dimerized tubulin lattice sites. We postulate that the microtubule is mostly uniform, dominated purely by GDP-bound dimers, and is capped by a disordered regime due to the presence of GTP-bound dimers as well. In the uniform region, we identify the electron hopping parameter regime in which the microtubule is a topological insulator. We then show the manner in which these topological features remain robust when the hopping parameters are disordered. We briefly mention possible biological implications for these microtubules to possess topologically robust electronic bound states.

Introduction. – Organic polymers and biomolecules have served as inspiration for discovering new condensed matter phenomena, with path-breaking insights developed for both biological systems and physical models [1,2]. The Su-Schrieffer-Heeger (SSH) model proposed in the 1980s for polyacetylene serves even today as a simple paradigm for topological phases of matter and charge fractionalization [3]. Such models have led to opening entire fields of study, bringing theoretical and experimental advances in our understanding of materials [4]. On the biological side, the fundamental units of the model, involving dimerization and sublattice symmetry, are building blocks for a range of complex macromolecules. Here, we investigate microtubules as a highly promising instance for extending such topological behavior in rich and diverse ways.

The microtubule is a protein complex that forms an integral part of the cellular cytoskeleton and consists of dimerized units arranged in a helical structure [5,6]. In ref. [7], the authors target the mechanical properties of these dimer units embedded in a manifold in the uniform (non-disordered) case and model the underlying interactions as harmonic coupling. The resulting dynamical equations show similarities with the Hamiltonian of topological insulators. Strikingly, the similarity translates to the mechanical system being topological —its phases are characterized by topological invariants and such regimes in parameter space possess classes of solutions reflecting signature end modes rendered robust by a spectral gap. As with metamaterials [8], the authors associate these modes with robust boundary phonon modes that play an important role in the growth and decay phases of microtubules. We do the same in a corresponding electronic system, and expect that the predicted phonon behavior in microtubules would imply corresponding analogues in its electronic properties.

In this work, we show that within a plausible parameter window, microtubules can possess a topological phase determined by their electronic band structure. On consideration of its electronic properties, we model it as

(a) E-mail: varshas2@illinois.edu (corresponding author)
(b) E-mail: smivish@illinois.edu

a cylindrical stack of SSH chains. We explore the properties of such quasi one-dimensional weak topological insulators and their response to disorder. We then discuss how these electronic phases map back to biological properties, possibly showing radically different kinds of conduction properties of microtubules stemming from the presence of topologically robust bound states.

The inherent complexity of biological systems is unavoidable in the attempt to build mathematical and physical models to describe them. While our model here is conceptual, we hope that it serves as a novel and sound hypothesis which can now be used to develop more complicated computational and experimental techniques to investigate the many unexplained processes in microtubules, where more conventional transport models are not enough to explain the biophysics at hand. Our model thus picks the simplest features of the microtubule that survive the complex nature of its surroundings —a dimer lattice with electron hopping— as a natural starting point.

Biophysics, structure, and electronic properties. – Microtubules play important roles in maintaining structural integrity of the cell, in initiating cellular mitosis, and in facilitating intracellular transport and signalling [9]. They are prominent structures in eukaryotic cells, especially crucial to the morphological makeup of neurons. The microtubule has also long been a popular candidate for the exploration of quantum effects manifesting in biological systems [10,11]. While it has often been argued that finite temperature and the environment associated with living cells would lead to decoherence and suppression of such effects, several recent studies provide evidence that they may not be ignored in several biological systems including microtubules [12–14]. Physiological temperature and solvent effects have even been theorized to aid rather than disrupt quantum mechanical effects in these systems in ref. [13]. While mesoscopic quantum coherence in microtubules remains controversial, there is growing evidence for the emergence of observable physical effects resulting from local quantum phenomena like electron tunnelling within proteins structures and specifically, microtubules [13,15–17]. In a more recent work [17], the authors obtain experimental evidence demonstrating that microtubules are, unexpectedly, effective light harvesters, which takes place through proximity of aromatic residues tryptophan and tyrosine in the microtubule. That is, quantum energy transfer can coherently diffuse across protofilaments for distances up to 6.6 nm, consistent with multistep hopping. Based on these works, we make the reasonable assumption that inter-tubulin electron tunnelling is a relevant process along microtubule filaments, which is fundamental to our work.

Structurally, the microtubule is a helical cylinder composed of tubulin units. These units are dimers consisting the homologous monomers α-tubulin and β-tubulin. Typically, the cylinders have a 25 nm outer diameter and 15 nm inner diameter. The dimers themselves have dimensions of 8 nm × 5 nm × 5 nm [18]. The dimers are attached helically around the cylinder giving rise to protofilaments, usually 13 in number around the circumference. The cylindrical lattice thus formed is highly ordered and is most commonly seen in two different configurations —with and without a prominent seam, corresponding to differences in helical pitch, as seen in fig. 1. As has been done with regards to mechanical properties in ref. [7], these cylinders can thus be modeled as extensions of the SSH system where the chain is wrapped around in a cylindrical configuration.

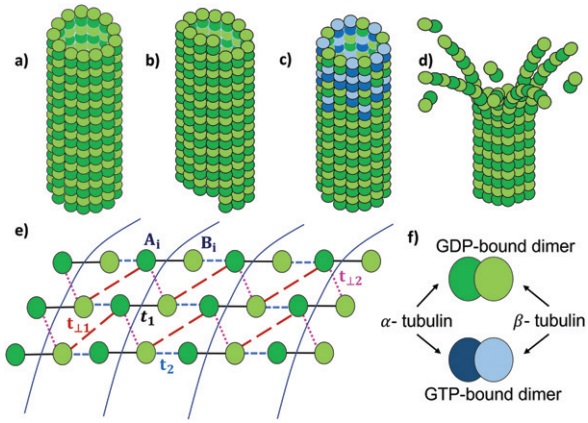

Fig. 1: The cylindrical microtubule is composed mainly of GDP-bound dimers (green). Panel (a) shows a microtubule of zero pitch, while (b) shows a microtubule having pitch equal to one dimer's length. Panels (c) and (d) show the microtubule in growth and decay phases respectively. While (a) and (b) are uniform, in (c), the "cap" of the microtubule has dimers of both the GDP and GTP (blue) kind, leading to increase in its length when more dimers from the surrounding medium attach onto the cap. This non-uniformity prevents the reduction in microtubule length, depicted in panel (d). Panel (e) shows the lattice model of the microtubule with associated hopping strengths. In panel (f) the α and β tubulin monomers are indicated in each type of dimer.

The microtubule shows two distinct phases when it undergoes "dynamic instability" —a growth or polymerization phase, where dimers from the surrounding solution attach themselves to the filaments of the microtubule, and a "peeling off" or de-polymerization phase, where the filaments of the microtubule curve outward longitudinally and lose dimers to the solution, decreasing the length of the tube [19,20]. The microtubule has been observed to stochastically switch between the two phases. The dimers can be of two possible types distinguished by the molecule attached at an exchange site —GDP or GTP. During the growth phase, dimers of both kinds attach themselves to the microtubule to form longer filaments. This non-uniform segment at the end of the tube is called the cap. As the tube grows, the GTP hydrolyzes to GDP after attachment to form uniform GDP attached

extended regions. The GDP-attached filaments are longitudinally curved, and it has been proposed that this curvature that results in the "peeling" off when the energetics overcome the stability provided by the cap [21,22]. Based on this structure of the microtubule, our model distinguishes two distinct regimes —one in the uniform GDP-based region, which we model as consisting of no disorder, and the other in the cap region, which we model as having a disorder distribution in the inter-tubulin charge hopping amplitudes.

Ample computational and observational studies indicate that the dimerized structure of the microtubule affects not only vibrational degrees of freedom, but also the intersite electronic hopping within the underlying lattice [23–26]. The conduction electron concentration on a microtubule has been estimated to be $n \sim 10^{19}\,\mathrm{cm}^{-3}$, which is higher than that of semiconductors, but significantly lower than that of metals. Even lower estimates of its conductivity from these numbers (at physiological temperatures) suggest a conductivity [18] that lies between $0.04\,\Omega^{-1}\ \mathrm{m}^{-1}$ and $10^5\,\Omega^{-1}\ \mathrm{m}^{-1}$. The microtubule has a large net negative charge per tubulin dimer that is mostly concentrated on the "C-terminus" of each dimer. The uncompensated negative charge is balanced in solution by counterions that screen the charge, giving rise to a dielectric polarization around the surface of the microtubule. This observation has led to several models of conductivity in terms of tight binding of electrons to the lattice site and effective charge hopping from site to site [18,26], like in the case of organic semiconductors [27,28]. Additionally, since the surrounding medium of the microtubule is rich in positively charged ions [24,29], the highly negatively charged microtubule might also exhibit conduction by proton hopping mechanisms, leading to higher conductivity, a phenomenon that plays a secondary role in this work. These descriptions for conductivity form the starting point of our analysis: we model electronic properties in terms of electrons hopping between nearest-neighbor lattice sites provided by the underlying α- and β-tubulin units.

Effective quasi-1D model. – Having established this tight-binding description for electron hopping between the α and β sites of the microtubule, we first analyze the uniform region. The resultant cylindrical lattice and hopping strengths are as depicted in fig. 1. The system consists of SSH chains along the length of the tube having alternating bond strengths t_1 and t_2. As shown in the figure, along the circumferential direction, the units are connected via bonds $t_{\perp,1}$ and $t_{\perp,2}$. Hubbard model treatments of the microtubule estimate these hopping strengths to be of the order 0.4–1 eV [18]. The pitch is reflected in the allowed quantized values of k_y. Here, due to the helical nature of the tubule, we assume that the staggering of the chains results in these inter-chain hoppings dominating. Thus, the predominant hopping terms respect sub-lattice symmetry in that hoppings are only between sub-lattices A consisting of α sites and B consisting of β sites, but not within each sublattice. The resultant Hamiltonian thus takes the generic form

$$H = \sum_{ij} \begin{pmatrix} c^\dagger_{A,ij} & c^\dagger_{B,ij} \end{pmatrix} \mathbb{H} \begin{pmatrix} c_{A,ij} \\ c_{B,ij} \end{pmatrix}, \tag{1}$$

where $\mathbb{H}$ obeys chiral symmetry such that $S\mathbb{H}S = -\mathbb{H}$ with $S = \sum_{ij}(c^\dagger_{A,ij}c_{A,ij} - c^\dagger_{B,ij}c_{B,ij})$. This Hamiltonian, emerging from the dominant hoppings, respects the symmetries of quasi-one-dimensional topological systems belonging to class AIII, classified as per the usual Altland-Zirnbauer formalism that characterizes topological systems according to their symmetries [30].

In the absence of inter-chain hopping, the paradigm SSH chains running along the length of the tube naturally support end bound states. These bound states correspond to robust mid-gap states in a spectrum symmetric about the Fermi energy having a gap of magnitude $|t_1 - t_2|$. Upon inter-chain coupling, qualitatively, these states too couple to form the end mode along the rim [31,32]; the robustness of similar states has been discussed in the context of coupled ladder systems [33–35]. Figures 2(b) and (c) plot such typical end-mode eigenstates in a regime that we have determined to be topological. For strong enough interchain coupling, the gap in the spectrum closes and the system undergoes a transition into a gapless phase where no such robust end-mode exists.

To analyze these features more rigorously, we express the Hamiltonian for a segment of this lattice in momentum space. To first order, we assume that the segment is long enough to take the thermodynamic limit. We assume a unit lattice constant for each bond. The resultant Hamiltonian takes the form

$$H = \begin{pmatrix} c^\dagger_{A,\vec{k}} & c^\dagger_{B,\vec{k}} \end{pmatrix} \begin{pmatrix} 0 & q(\vec{k}) \\ q^\dagger(\vec{k}) & 0 \end{pmatrix} \begin{pmatrix} c_{A,\vec{k}} \\ c_{B,\vec{k}} \end{pmatrix}, \tag{2}$$

where $q(\bar{k}) = u + ve^{-ik_x}$, $\bar{k} = (k_x, k_y)$, $u = t_1 + 2t_{\perp,2}\cos k_y$ and $v = 2t_{\perp,1}\cos k_y + t_2$. The energy band structure is given by $E_\pm = \pm\sqrt{u^2 + v^2 + 2uv\cos k_x}$.

In order to chart out the regimes where the system is topological in that a finite-sized tube would have end modes present, we can use the standard topological analysis of the band structure. In the thermodynamic limit, or under periodic boundary conditions in both directions, the band structure is gapped for a range of parameter regimes, as shown in the phase diagram in fig. 2. The gapped phases may further be classified as topological or trivial, as depicted in the phase diagram. Crucially, the topological phase is characterized by a topological invariant or winding number defined as

$$\nu_x = -\frac{i}{2\pi}\int \mathrm{d}k_x \mathrm{Tr}[q^{-1}\partial_{k_x} q]. \tag{3}$$

In this system, ν takes the value 1 for $|u| < |v|$ (topological) or 0 for $|u| > |v|$ (trivial) [4]. The system is gapless when $|u| = |v|$.

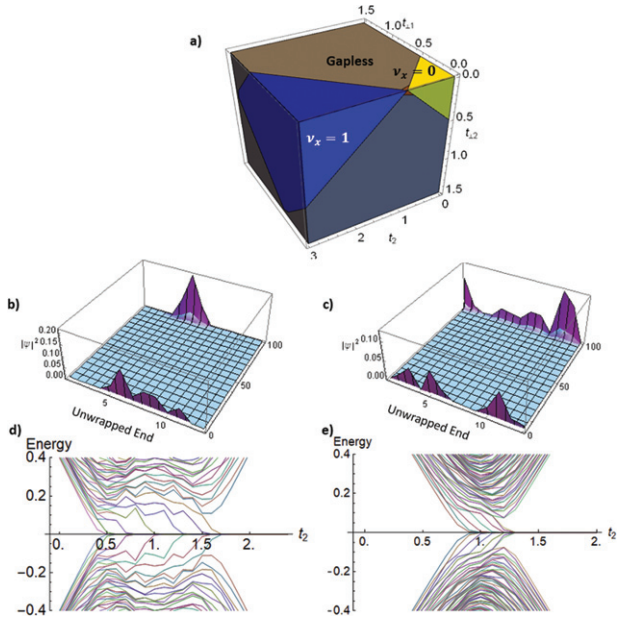

Fig. 2: Energy bands and phase diagram: Panel (a) shows the phase diagram for the lattice model under the thermodynamic limit, as a function of hopping strengths t_2, $t_{\perp,1}$ and $t_{\perp,2}$ all scaled to be in units of t_1. The gapless and gapped phases are indicated, with the gapped phases being identified by their associated topological invariant. Panels (b) and (c) show one of the possible zero energy edge states for a cylindrical strip of $N_y = 13$ chains with 50 dimers along the length of the microtubule in the topological phase. Panel (b) is for a helical cylinder of pitch zero, while (c) is for a helical cylinder with unit pitch. Panels (d) and (e) demonstrate the changes in the band structure for strip of pitch zero (panel (d)) and pitch one (panel (e)) when the parameter t_2 is tuned from 0 to 3. Here, $t_{\perp,1} = 0.2$ and $t_{\perp,2} = 0.1$. The figure shows an initial configuration with a trivial gap become gapless for a range of values before again opening up a topological gap. The zero energy modes are also seen in the topological gap.

The band structure of a finite cylindrical strip is shown in figs. 2(d) and (e), for two different boundary conditions of the microtubule. In the figures, as parameter t_2 is increased, it is seen that that system initially has a trivial gap, and then passes through a regime of gaplessness before opening up a topological gap, distinguished by the presence of zero energy edge states. For a cylindrical strip of N_y chains, there are $2N_y$ zero energy modes in the gap, in the absence of sub-lattice symmetry-breaking terms. In our quasi-1D model, this situation corresponds to a topological invariant $\nu_x = 1$ (higher integers are usually associated with long-range coupling in such conjugated systems). These edge states can then couple with other systems, hybridize with each other for short enough tube lengths, or interact with environmental modes. These effects give rise to a host of phenomena that have been extensively studied in the context of SSH chains and would be of direct relevance to microtubules [36–38]. Moreover, while the staggered helical nature of the microtubule allows the reasonable assumption of low hoppings of the kind A-A or B-B or non-uniform on-site chemical potential, their presence explicitly breaks the aforementioned sublattice symmetry of the system. For small values of such symmetry breaking terms (with respect to the gap), the spectrum is shifted or stretched or both, thus lifting some or all the edge states from zero energy [39]. However, they retain their topological significance despite due to the presence of the gap. Very high values, on the other hand, can close the gap and cause these edge states to become absent.

Disorder and dynamic instability. – The growth phase of the microtubule sets in when the ends are not uniformly composed of GDP dimers, but also contain interspersed GTP dimers. Further, in some diseased states, there could also be isoforms of tubulin present, which would further contribute to the non-uniformity of the cap [40]. This non-uniformity can be reasonably expected to affect the electron hopping strength. Moreover, given that the GTP molecules are in metastable stages of hydrolysis enroute to conversion to GDP, we expect a continuous range of non-uniformity, as opposed to a binary distribution. A full treatment of such effects involves considerations of dynamics and energetics as brought about by these changes. As a preliminary step, however, we treat these changes as non-uniformities in the lattice. We model such non-uniformity in the cap as disorder in the hopping parameters, and characterize its effects on topological properties via changes made to the winding number.

Since the cap does not cover the entire length of the microtubule, we assume disorder only in part of the tube. As a specific proof-of-principle instance, we model the presence of disorder in half the tube. In order to determine the phase of the microtubule, we employ the real space version of the topological invariant typically used for disordered systems [41–43]. To briefly provide the recipe, in the basis of eigenstates of S, the Hamiltonian can be written in the off-diagonal form of eq. (2). One then defines a "flat-band" version Q of this real-space Hamiltonian as $Q = P_+ - P_-$, where $P_\pm$ are projectors onto eigenspaces with positive and negative eigenvalues. The invariant is given by

$$\nu = -\frac{1}{N_x}\mathrm{Tr}(\tilde{Q}^\dagger[X,\tilde{Q}]), \qquad Q = \begin{pmatrix} 0 & \tilde{Q} \\ \tilde{Q}^\dagger & 0 \end{pmatrix}. \tag{4}$$

Here N_x is the number of unit cells along the lattice and X is the position operator in the lattice.

Our model of the microtubule corresponds to the AIII class of topological insulators.

We effectively evaluate the topological invariant per unit width $\nu_x = \nu/N_y$ where N_y is the number of protofilaments. Thus, ν_x is quantized in units of $1/N_y$. This quantized behaviour has been established both analytically and numerically, even in the presence of strong disorder [42]. In our system, we apply disorder to the hopping strengths t_1 and t_2 individually. For each of these hopping strengths

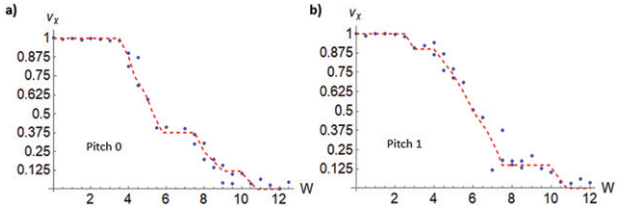

Fig. 3: Topological invariant ν_x plotting against disorder strength W in t_1 and strength $W/2$ in t_2 for $N_y = 8$ in two possible pitch configurations. The blue points correspond to the real space topological invariant for a microtubule of pitch zero, and the red curve is a rough fit of the data points. The initial quantization is briefly retained until $W \sim 3$.

h_i, disorder is applied through the equation $h_i = h_{i0} + W_i u$ where u is a uniform random variable sampled between $[-0.5, 0.5]$ and W_i is the strength of the disorder. The initial parameters h_{i0} are picked so that the microtubule starts at a topological phase. We also pick $W_1 = W$ for t_1 and $W_2 = W/2$ for t_2. These parameters represent a typical sample which demonstrates the plausible evolution of topological features.

The results thus obtained are shown in fig. 3. A few caveats are in order. The trend clearly shows a nearly quantized value of unity for the invariant at low disorder that drops towards zero upon increasing disorder. The curve can stabilize at other values of ν_x that are multiples of $1/N_y$. Fluctuations around the allowed values are a result of the finite size of the system chosen and diminish for longer systems [42]. We expect out results to hold for the more realistic number $N_y \sim 13$. While the form of the invariant assumes sublattice symmetry, we expect the topological feature of a robust edge mode to remain for small deviations from this symmetry condition. Most importantly, the simulation is a demonstration of the salient properties in the presence of disorder. Our simulations show that the quantization is retained for values of disorder as high as $W = 3$. While this treatment considers the segment as a whole, with disorder in half the region to represent the physical situation, a more detailed analysis would show the exact physical location of the end modes as possibly shifting into the interior. Most prominently, we may reasonably expect that for regions of lower disorder, the presence of the edge mode would still be prevalent.

Discussion and outlook. – Here, we have given a proof-of-concept presentation of how topological properties of tight-binding lattices, emerging from their electronic conductivity properties, can provide microtubules with unique bound state structure hitherto unexplored. It adds to a growing body of work that posits coherent transport of quantum excitations across microtubules even in physiological conditions, like in refs. [13,18,26], etc. Here, we associate the decay and growth phases of the microtubule with the presence or disorder-induced vanishing of an electronic topological edge mode. Realistically, several variations of our model could come into play including the effects of environmental interactions, and the non-equilibrium stochastic nature of microtubule growth. In particular, the estimated hopping strengths in previous works [18] indicate a gap energy of the order of 0.4–1 eV, which is much higher than physiological temperatures. While this could heuristically indicate that the topological gap is robust to thermal excitations, a more rigorous treatment of the system in interaction with thermal vibrational modes and other environmental factors is needed, which is beyond the scope of this current work. Further, in this work, we assumed sublattice symmetry, which ultimately gives rise to the mid-gap states centered at the Fermi energy. We expect that deviations either due to on-site potential variations or other couplings within each of the A and B sublattices would still preserve the edge modes for values small enough in comparison to the dimer bond strength. Additionally, one could adapt these calculations to extremely short microtubules as they start to grow out of the centrosome, and perhaps to extremely long microtubules that push an embryonic neuronal cell membrane out to grow towards future synapses.

While our model is phenomenological in nature, further studies would connect the disorder distribution to physical conditions, such as hydrolysis states, temperature effects, microtubule-associated proteins, such as kinesin and dynein and presence of other biochemicals. Moreover, while we studied uniform *vs.* disordered behavior for entire segments, it is possible to have more robust bound states at the interface of such segments. Nevertheless, the presence of topologically robust modes in the microtubule is further supported by studies of isotypes of tubulin in diseased microtubules. It is seen that their functioning is only marginally altered, with such defects only becoming apparent in processes that are highly sensitive to microtubule dynamics [44]. A further intriguing possibility would involve possible coupling between such edge modes posited by mechanical and electronic degrees of freedom.

Finally, the existence of robust edge state modes could have significant biological implications. In principle, the bound state could act as an acceptor or donor of charge, perhaps differentially influencing the more negatively charged GTP compared with the GDP molecule. Considering their role in neural transmission, they may also extend into various parts of the axon terminal, and dynamically change the open-or-closed states of voltage-gated ion channels, contributing to pre-synaptic membrane activity. Conversely, proteins that have an overall positive charge or neurite regions that have a concentration of positive charge (such as an action potential's influx of cations) might attract the microtubule if it is in the topological regime for hosting negative charge at its end. Regardless of the extent to which microtubules are involved with intra-neuronal activity besides transport [10,11], it is likely that sub-neuronal computation is an important part of brain function, and microtubules

may play a significant role in that. As in condensed matter systems, conduction properties of microtubules hinge greatly on their structure, chemical composition and environment; their possible behavior as topological insulators may bear radical insights into the quantum nature of biophysical systems.

* * *

We thank Camelia Prodan and Emil Prodan for sharing beautiful insights both in their work and through conversations. We also thank Kesav Krishnan for useful conversations. We acknowledge the support of the National Science Foundation under grants DMR-2004825 (VS and SmV) and CAREER DMS-1254791 (KLK). As an Honorary Scientist, SaV acknowledges the National Academy of Sciences, India (NASI).

Data availability statement: The data that support the findings of this study are available upon reasonable request from the authors.

REFERENCES

[1] Spakowitz A. J., *J. Chem. Phys.*, **151** (2019) 230902.
[2] Alvarez-Estrada R. F. and Calvo G. F., *Mol. Phys.*, **100** (2002) 2957.
[3] Su W. P., Schrieffer J. R. and Heeger A. J., *Phys. Rev. B*, **22** (1980) 2099.
[4] Asbóth J. K., Oroszlány L. and Pályi A., *Lecture Notes in Physics*, vol. **919**, (Springer, Cham) 2016, DOI: 10.1007/978-3-319-25607-8.
[5] Wade R. H., *Mol. Biotechnol.*, **43** (2009) 177.
[6] Amos L. A., *Semin. Cell. Dev. Biol.*, **22** (2011) 916.
[7] Prodan E. and Prodan C., *Phys. Rev. Lett.*, **103** (2009) 248101.
[8] Xin L., Siyuan Y., Harry L., Minghui L. and Yanfeng C., *Curr. Opin. Solid State Mater. Sci.*, **24** (2020) 100853.
[9] Avila J., *Life Sci.*, **50** (1992) 327.
[10] Hameroff S. R. and Watt R. C., *J. Theor. Biol.*, **98** (1982) 549.
[11] Hameroff S. and Penrose R., *Math. Comput. Simul.*, **40** (1996) 453.
[12] Marais A., Adams B., Ringsmuth A. K., Ferretti M., Gruber J. M., Hendrikx R., Schuld M., Smith S. L., Sinayskiy I., Krger T. P. J., Petruccione F. and van Grondelle R., *J. R. Soc. Interface*, **15** (2018) 20180640.
[13] Craddock T. J. A., Friesen D., Mane J., Hameroff S. and Tuszynski J. A., *J. R. Soc. Interface*, **11** (2014) 20140677.
[14] Mavromatos N. E. and Nanopoulos D. V., *Int. J. Mod. Phys. B*, **12** (1998) 517.
[15] Sahu S., Ghosh S., Fujita D. and Bandyopadhyay A., *Sci. Rep.*, **4** (2014) 7303.
[16] Gray H. B. and Winkler J. R., *Quart. Rev. Biophys.*, **36** (2003) 341.
[17] Kalra A. P., Benny A., Travis S. M., Zizzi E. A., Morales-Sanchez A., Oblinsky D. G., Craddock T. J. A., Hameroff S. R., MacIver M. B., Tuszyński J. A., Petry S., Penrose R. and Scholes G. D., *ACS Centr. Sci.*, **9** (2023) 352.
[18] Tuszynski J. A., Priel A., Brown J. A., Cantiello H. F. and Dixon J. M., *Nano and Molecular Electronics Handbook* (CRC Press) 2018.
[19] Brouhard G. J., *Mol. Biol. Cell*, **26** (2015) 1207.
[20] Horio T. and Murata T., *Front. Plant Sci.*, **5** (2014) 511.
[21] Burbank K. S. and Mitchison T. J., *Curr. Biol.*, **16** (2006) R516.
[22] Brun L., Rupp B., Ward J. J. and Nédélec F., *Proc. Natl. Acad. Sci. U.S.A.*, **106** (2009) 21173.
[23] Eakins B. B., Patel S. D., Kalra A. P., Rezania V., Shankar K. and Tuszynski J. A., *Front. Mol. Biosci.*, **8** (2021) 150.
[24] Tuszynski J. A., *The bioelectric circuitry of the cell*, in *Brain and Human Body Modelling: Computational Human Modeling at EMBC 2018*, edited by Makarov S., Horner M. and Noetscher G. (Springer International Publishing, Cham) 2019, pp. 195–208.
[25] Minoura I. and Muto E., *Biophys. J.*, **90** (2006) 3739.
[26] Nganfo W., Kenfack-Sadem C., Fotué A., Ekosso M., Wopunghwo S. and Fai L., *Heliyon*, **8** (2022) e08897.
[27] Rühle V., Lukyanov A., May F., Schrader M., Vehoff T., Kirkpatrick J., Baumeier B. and Andrienko D., *J. Chem. Theory Comput.*, **7** (2011) 3335.
[28] Kirkpatrick K., Lenzmann E. and Staffilani G., *Commun. Math. Phys.*, **317** (2013) 563.
[29] Eakins B. B., Patel S. D., Kalra A. P., Rezania V., Shankar K. and Tuszynski J. A., *Front. Mol. Biosci.*, **8** (2021) 150.
[30] Schnyder A. P., Ryu S., Furusaki A. and Ludwig A. W. W., *AIP Conf. Proc.*, **1134** (2009) 10.
[31] Delplace P., Ullmo D. and Montambaux G., *Phys. Rev. B*, **84** (2011) 195452.
[32] Zhu L., Prodan E. and Ahn K. H., *Phys. Rev. B*, **99** (2019) 041117.
[33] Li C., Lin S., Zhang G. and Song Z., *Phys. Rev. B*, **96** (2017) 125418.
[34] Hügel D. and Paredes B., *Phys. Rev. A*, **89** (2014) 023619.
[35] Padavić K., Hegde S. S., DeGottardi W. and Vishveshwara S., *Phys. Rev. B*, **98** (2018) 024205.
[36] Lieu S., McGinley M. and Cooper N. R., *Phys. Rev. Lett.*, **124** (2020) 040401.
[37] McGinley M. and Cooper N. R., *Phys. Rev. Res.*, **1** (2019) 033204.
[38] Campos Venuti L., Ma Z., Saleur H. and Haas S., *Phys. Rev. A*, **96** (2017) 053858.
[39] Pérez-González B., Bello M., Gómez-León A. and Platero G., *Phys. Rev. B*, **99** (2019) 035146.
[40] Vemu A., Atherton J., Spector J. O., Moores C. A. and Roll-Mecak A., *Mol. Biol. Cell*, **28** (2017) 3564.
[41] Prodan E., *J. Phys. A: Math. Theor.*, **44** (2011) 113001.
[42] Claes J. and Hughes T. L., *Phys. Rev. B*, **101** (2020) 224201.
[43] Mondragon-Shem I., Hughes T. L., Song J. and Prodan E., *Phys. Rev. Lett.*, **113** (2014) 046802.
[44] Gadadhar S., Bodakuntla S., Natarajan K. and Janke C., *J. Cell Sci.*, **130** (2017) 1347.